Two-Fluid Flowing Equilibria of Helicity Injected Spherical Torus with Non-Uniform Density

Takashi KANKI, Loren C. STEINHAUER[1)] and Masayoshi NAGATA[2)]

Department of Maritime Science and Technology, Japan Coast Guard Academy, Kure, Hiroshima 737-8512, Japan

[1)]*University of Washington, Redmond Plasma Physics Laboratory, Redmond, Washington 98052, USA*

[2)]*Department of Electrical Engineering and Computer Sciences, University of Hyogo, Himeji, Hyogo 671-2201, Japan*

Two-dimensional two-fluid flowing equilibria of helicity-injected spherical torus with non-uniform density and both toroidal and poloidal flows for each species have been numerically determined by means of the nearby-fluids procedure. It is found from the numerical results that the equilibrium for the driven λ ($\equiv \mu_0\, \boldsymbol{j} \cdot \boldsymbol{B} / B^2$) profile has a diamagnetic toroidal field, high-β (toroidal beta value, $\beta_t = 32\%$), hollow current profile, and centrally broad density. By contrast, the decaying equilibrium has a paramagnetic toroidal field, low-β ($\beta_t = 10\%$), centrally peaked current profile, and density with a steep gradient in the outer edge region. In the driven case, the toroidal ion and electron flows are in the same direction, and two-fluid effects are less important since the $\boldsymbol{E} \times \boldsymbol{B}$ drift is dominant. In the decaying case, the toroidal ion and electron flows are opposite in the outer edge region, and two-fluid effects are significant locally in the edge due to the ion diamagnetic drift.

Keywords: helicity injection, equilibrium, plasma flow, two-fluid effect, $\boldsymbol{E} \times \boldsymbol{B}$ drift, diamagnetic drift

1. Introduction

Many experiments on current drive of spherical torus using a coaxial helicity injection (CHI) have been performed to elucidate the current drive mechanism for CHI. In these experiments, $\boldsymbol{E} \times \boldsymbol{B}$ plasma toroidal rotation with an n=1 kink mode the during CHI has been observed. It is recognized that the effect of plasma flow is important in understanding the confinements and relaxed states of helicity-injected spherical torus (HI-ST) plasmas. Especially, in the Helicity Injected Torus-II (HIT-II) experiments, a rotating n=1 magnetic structure observed at the outer plasma edge is locked to the electron fluids and not to the ion fluids, suggesting a rotating magnetic field current drive [1]. Because of this behavior, the equilibrium computation of the HI-ST is required to take into account two-fluid effects [2,3]. The formalism for two-fluid flowing equilibria was developed [4], and two-dimensional equilibria in helicity-driven systems using the two-fluid model were previously computed, showing the existence of an ultra-low-q spherical torus configuration with diamagnetism and higher beta [5]. However, this computation assumed purely toroidal ion flow and uniform density. The purpose of this study is to apply the two-fluid model to the two-dimensional equilibria of HI-ST with non-uniform density and both toroidal and poloidal flows for each species by means of the nearby-fluids procedure [6], and to explore their properties. We focus our attention on the equilibria relevant to the Helicity Injected Spherical Torus (HIST) device, which are characterized by either driven or decaying λ ($\equiv \mu_0\, \boldsymbol{j} \cdot \boldsymbol{B} / B^2$) profiles [7]. Here μ_0, $\boldsymbol{j}$, and $\boldsymbol{B}$ are the permeability of vacuum, current density, magnetic field. We have qualitatively reproduced the HIST equilibria in the driven or decaying λ profiles on the basis of the experimental data such as λ, $\boldsymbol{j}$, and $\boldsymbol{B}$ profiles.

2. Governing Equations

Let us assume axisymmetry about HIST geometric axis in cylindrical coordinates (r, θ, z). Hereafter all variables are dimensionless [6]. An axisymmetric two-fluid flowing equilibrium is described by a pair of generalized Grad-Shafranov equations for ion surface variable $\Upsilon(r, z)$ and electron surface variable $\psi(r, z)$ [6],

$$\overline{\psi}_i' r^2 \nabla \cdot \left(\frac{\overline{\psi}_i'}{n} \frac{\nabla \Upsilon}{r^2} \right) = \frac{r}{\varepsilon}\left(B_\theta \overline{\psi}_i' - n u_\theta \right) + n r^2 \left(H_i' - T_i S_i' \right), \quad (1)$$

$$r^2 \nabla \cdot \left(\frac{\nabla \psi}{r^2} \right) = \frac{r}{\varepsilon}\left(B_\theta \overline{\psi}_e' - n u_\theta \right) - n r^2 \left(H_e' - T_e S_e' \right), \quad (2)$$

and a generalized Bernoulli equations for the density n,

$$\frac{\gamma}{\gamma - 1} n^{\gamma-1} \exp\left[(\gamma - 1) S_i \right] + \frac{u^2}{2} + \phi_E = H_i, \quad (3)$$

$$\frac{\gamma}{\gamma - 1} n^{\gamma-1} \exp\left[(\gamma - 1) S_e \right] - \phi_E = H_e. \quad (4)$$

Here $\boldsymbol{u}$, T_α, ε, ϕ_E, and γ are the ion flow velocity, species (α=i, e) temperature, two-fluid parameter, electrostatic potential, and adiabatic constant, respectively. Note that ε value is 0.0625 in the HIST experiment, and that $\psi(r, z)$

author's e-mail: kanki@jcga.ac.jp

corresponds to the familiar poloidal flux function. The poloidal flow stream function $\overline{\psi}_\alpha$, total enthalpy function H_α and entropy function S_α are arbitrary surface functions of their respective surface variables. The three arbitrary functions $\Lambda_\alpha(\equiv \overline{\psi}'_\alpha)$, H_α, and S_α for each species can be assumed so as to reflect λ, $\boldsymbol{j}$, and $\boldsymbol{B}$ profiles on the basis of the experimental data by choosing appropriate function forms,

$$\Lambda_i(\mathrm{Y}) = \Lambda_{i0} + (\Lambda_{i1} - \Lambda_{i0})\left.\frac{df}{dx}\right|_{\mathrm{Y}-\Delta\mathrm{Y};\delta_{i1},\delta_{i2}}, \tag{5}$$

$$\Lambda_e(\psi) = \Lambda_{e0} + (\Lambda_{e1} - \Lambda_{e0})\left.\frac{df}{dx}\right|_{\psi-\Delta\psi;\delta_{e1},\delta_{e2}}, \tag{6}$$

$$f(x;\delta_1,\delta_2) = \frac{1}{\delta_1+\delta_2} \times \begin{Bmatrix} \delta_1^2 \exp[x/\delta_1]; \quad x<0 \\ \delta_1 x + \delta_2\sqrt{\delta_2^2+x^2} - \delta_2^2 + \delta_1^2;\ x \geq 0 \end{Bmatrix}. \tag{7}$$

Here $\Lambda_{\alpha0}$, $\Lambda_{\alpha1}$, $\delta_{\alpha0}$, $\delta_{\alpha1}$, $\Delta\mathrm{Y}$, and $\Delta\psi$ are constant parameters. By adjusting these constant parameters, we can obtain the driven or decaying λ profiles. Other arbitrary functions H_α and S_α are the same function form as Λ_α.

Equations (1) and (2) have terms of order $1/\varepsilon$ on the right-hand side, and they cause singularities. We employ the nearby-fluids procedure to eliminate the singularities [6]. This procedure requires that two arbitrary functions Λ_i and Λ_e must differ only to $O(\varepsilon)$. We consider replacing these two arbitrary functions with a pair of arbitrary functions F and G expressed as follows:

$$\Lambda_e(\psi) = F(\psi), \quad \Lambda_i(\mathrm{Y}) = F(\mathrm{Y}) + \varepsilon G'(\mathrm{Y}). \tag{8}$$

Note that G and Λ_e correspond to the toroidal field function and the familiar Taylor $\lambda(\psi)$ function, respectively. Therefore, the toroidal field with $GG' > 0$ gives a paramagnetic profile, while that with $GG' < 0$ gives a diamagnetic one.

Next, we consider the boundary conditions for Eqs. (1)-(4). No magnetic flux penetrates the flux conserver (FC). Therefore, ψ is fixed at 0 at the FC wall. The bias flux is given by assigning fixed values of ψ to grid points corresponding to the entrance port of the FC. These values are calculated using the formula,

$$\psi_{\mathrm{bias}}(r) = \frac{4\psi_s}{(R_e - R_c)^2}(r-R_c)(R_e-r), \tag{9}$$

where R_c, R_e, and ψ_s are the radius of the central conductor, that of the entrance port, and the maximum value of the bias flux, respectively. A toroidal field coil current along the geometry axis inside the central conductor produces a vacuum toroidal field $B_{t.v}$. The effect of $B_{t.v}$ is inserted by G_0 in

$$G(\mathrm{Y}) = G_0 + \frac{1}{\varepsilon}\left[\int \Lambda_i(\mathrm{Y})d\mathrm{Y} - \int \Lambda_e(\psi)d\psi\right]. \tag{10}$$

Under the above assumptions and boundary conditions, the equilibrium is numerically determined by using a successive over-relaxation method for updating the poloidal flux function and a Newton-Raphson method for updating the density.

3. Numerical Results

We investigate the fundamental properties of the HIST equilibria in the driven or decaying λ profiles. The radial profiles of the magnetic structure at the midplane are shown in Fig. 1. In the driven λ profile, the toroidal field B_t has a diamagnetic profile due to the condition $GG' < 0$, and the toroidal beta value β_t is high (β_t = 32%). The condition means $\Lambda_e > \Lambda_i$ and then reflects that the absolute value of electron flow velocity is larger than that of ion flow velocity. The poloidal field B_z is much smaller than B_t and is almost flat in the core region. The toroidal current density j_t has a hollow profile and almost zero in the core region. In the decaying λ profile, B_t has a paramagnetic profile except for the inner edge region, and β_t is low (β_t = 10%). Also, j_t has a centrally peaked profile with a slightly outward shift.

The radial profiles of the plasma structure at the midplane are shown in Fig. 2. In the driven λ profile, the density n is a centrally broad profile. Both ion temperature T_i and electron temperature T_e have flat profiles, and their magnitudes are almost same. The electrostatic potential ϕ_E

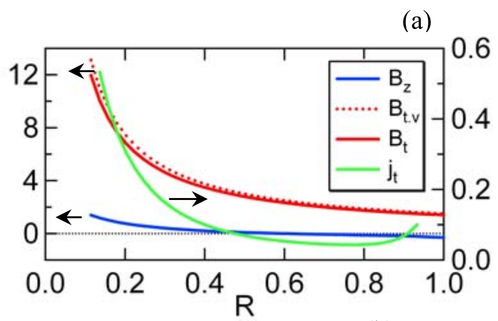

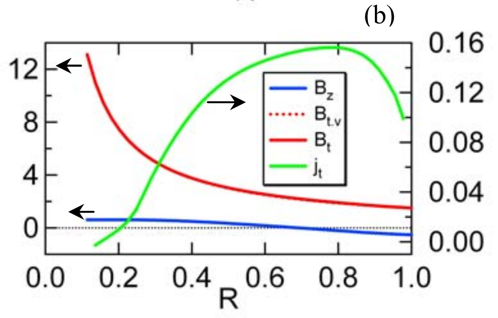

Fig.1 Radial profiles of the magnetic field and toroidal current density at the midplane; (a) driven λ profile and (b) decaying λ profile.

is peaked towards the periphery region, and reflects that the electric field is applied by the coaxial helicity source (CHS). In the decaying λ profile, n is a centrally peaked profile. Both T_i and T_e have similarly peaked profiles, and their magnitudes are almost same. Also, ϕ_E has almost flat profile which reflects that the electric field is hardly applied by the CHS.

The radial profiles of the flow structure at the midplane are shown in Fig. 3. In the driven λ profile, the electron toroidal flow velocity u_{et} is larger than the ion one u_{it}, and u_{it} and u_{et} are in the same direction. Both toroidal and poloidal electron flow velocities rise up sharply near the inner edge region and cause the hollow current profile. In the decaying λ profile, u_{it} is larger than u_{et} except for the inner edge region, and u_{it} and u_{et} are opposite in the outer edge region.

We investigate the generalized Ohm's law,

$$\begin{aligned} &\boldsymbol{E} + (1/\varepsilon)\boldsymbol{u}\times\boldsymbol{B} + \boldsymbol{F}_{2F} = 0, \\ &\boldsymbol{F}_{2F} = -\nabla p_i / n - \boldsymbol{u}\cdot\nabla\boldsymbol{u}. \end{aligned} \tag{11}$$

Here $\boldsymbol{E}$ and $\boldsymbol{F}_{2F}$ express the electric field and two-fluid effect, respectively. The terms $-\nabla p_i / n$ and $-\boldsymbol{u}\cdot\nabla\boldsymbol{u}$ cause the ion diamagnetic and inertial effects, respectively. The radial profiles of $\boldsymbol{E}$, $(1/\varepsilon)\boldsymbol{u}\times\boldsymbol{B}$, $\boldsymbol{F}_{2F}$, $-\nabla p_i / n$, and $-\boldsymbol{u}\cdot\nabla\boldsymbol{u}$ at the midplane are shown in Fig. 4. All components are radial. In the driven λ profile, the two-fluid effect is not so large except for both edge regions. The ion diamagnetic and inertial effects are relatively large both edge regions, but they are in the opposite direction. In the decaying λ profile, the two-fluid effect is dominant in the outer edge region due to the ion diamagnetic effect.

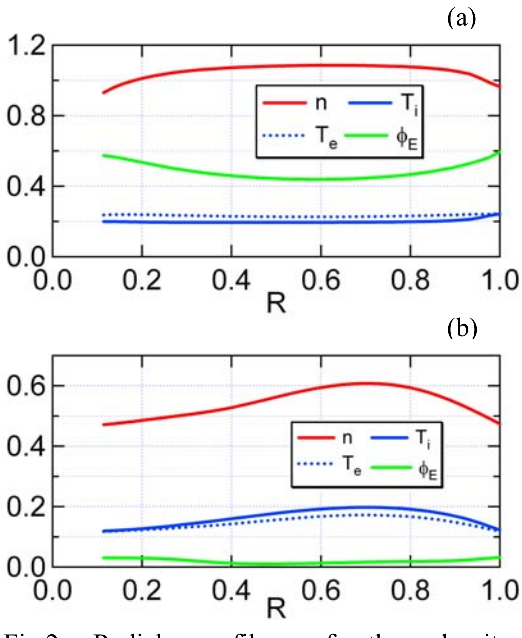

Fig.2 Radial profiles of the density, temperatures and electrostatic potential at the midplane; (a) driven λ profile and (b) decaying λ profile.

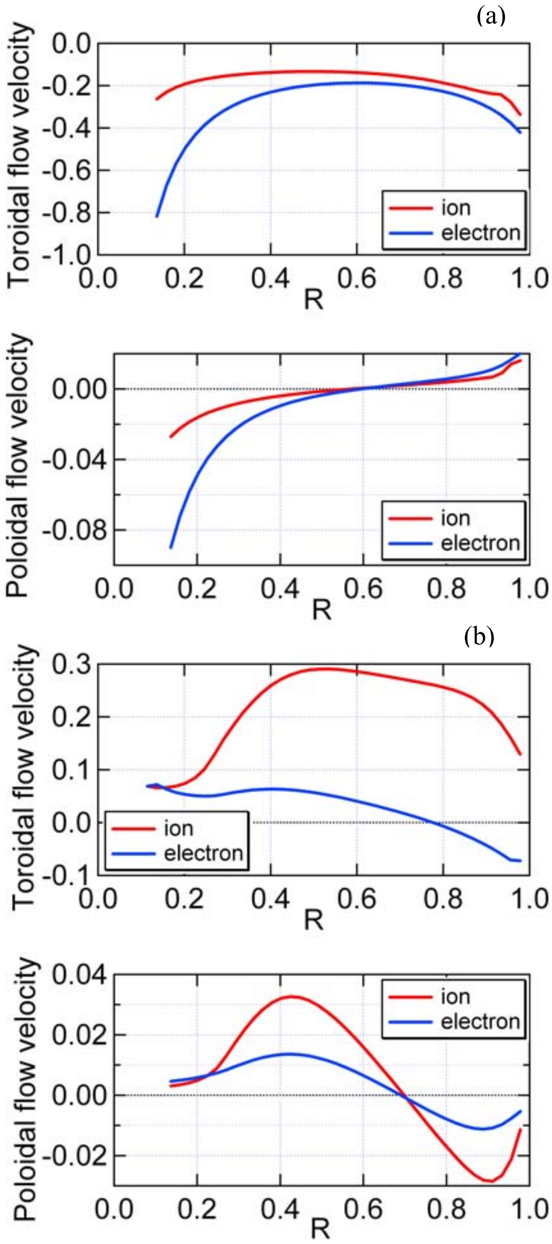

Fig.3 Radial profiles of the toroidal and poloidal flow velocities at the midplane; (a) driven λ profile and (b) decaying λ profile.

The radial profiles of the ion drift velocity at the midplane are shown in Fig. 5. In the driven λ profile, the $\boldsymbol{E}\times\boldsymbol{B}$ drift velocity is dominant. This velocity is the same direction as the toroidal ion flow one, but is the opposite direction to the toroidal current density. This result is consistent with the observation in the HIST and other CHI experiments. In the decaying λ profile, the ion diamagnetic drift velocity is dominant. This velocity is the same direction as the toroidal ion flow one, but is the opposite direction to the $\boldsymbol{E}\times\boldsymbol{B}$ one.

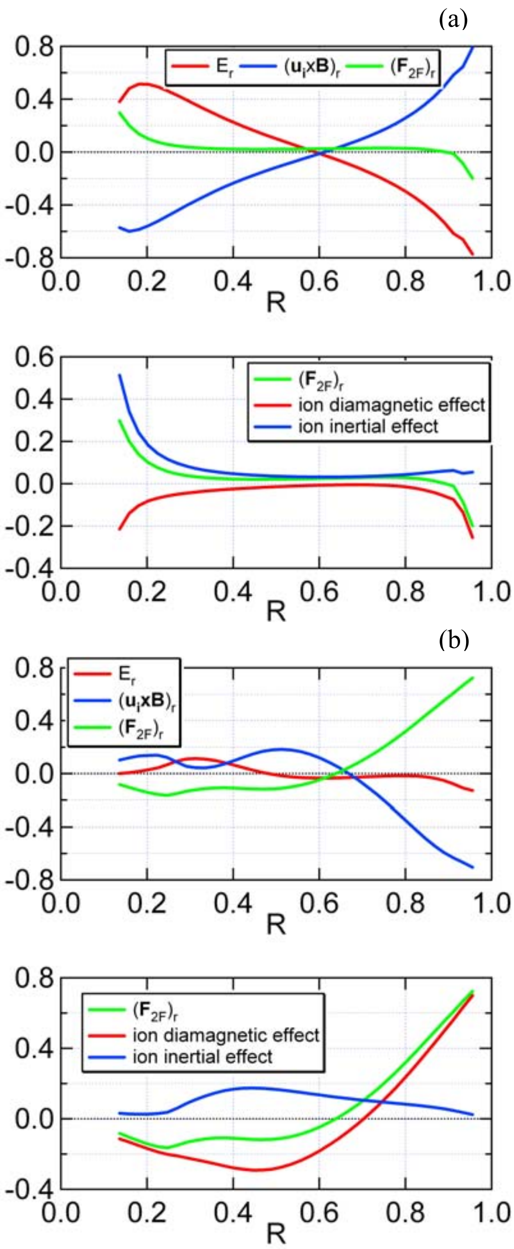

Fig.4 Radial profiles of $\boldsymbol{E}$, $(1/\varepsilon)\boldsymbol{u}\times\boldsymbol{B}$, $\boldsymbol{F}_{2F}$, $-\nabla p_i/n$, and $-\boldsymbol{u}\cdot\nabla\boldsymbol{u}$ at the midplane; (a) driven λ profile and (b) decaying λ profile. All components are radial.

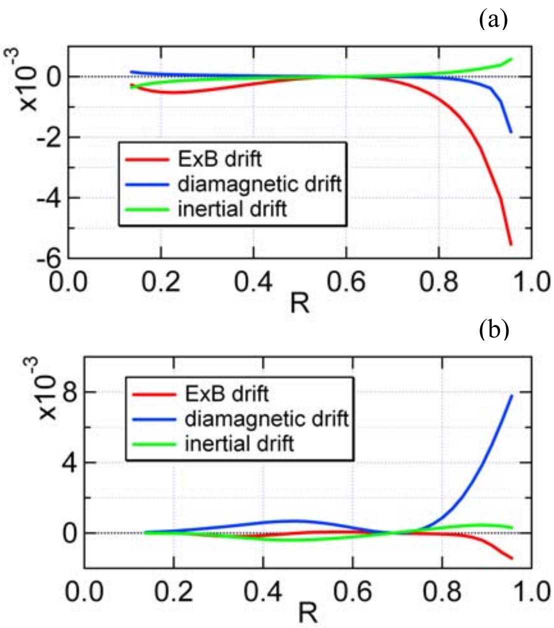

Fig.5 Radial profiles of the ion drift velocity at the midplane; (a) driven λ profile and (b) decaying λ profile. All components are toroidal.

3. Summary and Conclusions

We have computed the two-dimensional two-fluid flowing equilibria with non-constant density and the poloidal as well as toroidal flows for each species by using the nearby-fluids procedure. We focus our attention on the HI-ST equilibria relevant to the HIST device, which are characterized by either driven or decaying λ profiles, and explore their properties. Conclusions are summarized as follows. 1) In the driven λ profile, the equilibrium has the diamagnetic toroidal field, high-β (β_t=32%), hollow current profile, and centrally broad density. The toroidal ion and electron flows are in the same direction, and two-fluid effects are less important since the $\boldsymbol{E}\times\boldsymbol{B}$ drift is dominant. 2) In the decaying λ profile, the equilibrium has the paramagnetic toroidal field, low-β (β_t=10%), centrally peaked current profile, and density with the steep gradient in the outer edge region. The toroidal ion and electron flows are opposite in the outer edge region, and two-fluid effects are significantly locally in the edge due to the ion diamagnetic drift.

[1] K.J. McCollam and T.R. Jarboe, Plasma Phys. Control. Fusion **44**, 493 (2002).
[2] L.C. Steinhauer and A. Ishida, Phys. Rev. Lett. **79**, 3423 (1997).
[3] Z. Yoshida and S.M. Mahajan, Phys. Rev. Lett. **88**, 095001 (2002).
[4] L.C. Steinhauer, Phys. Plasmas **6**, 2734 (1999).
[5] T. Kanki and M. Nagata, Phys. Plasmas **13**, 072506 (2006).
[6] L.C. Steinhauer and A. Ishida, Phys. Plasmas **13**, 052513 (2006).
[7] M. Nagata, T. Kanki, N. Fukumoto and T. Uyama, Phys. Plasmas **10**, 2932 (2003).